Neurobiology of Disease 191 (2024) 106393

Contents lists available at ScienceDirect

Neurobiology of Disease

journal homepage: www.elsevier.com/locate/ynbdi

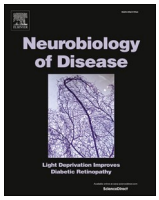

Defects in AMPAR trafficking and microglia activation underlie socio-cognitive deficits associated to decreased expression of phosphodiesterase 2 a

Sébastien Delhaye [a], Marielle Jarjat [a], Asma Boulksibat [a], Clara Sanchez [a], Alessandra Tempio [a], Andrei Turtoi [b], Mauro Giorgi [c], Sandra Lacas-Gervais [d], Gabriele Baj [e], Carole Rovere [a], Viviana Trezza [f], Manuela Pellegrini [c,g], Thomas Maurin [a,1], Enzo Lalli [a], Barbara Bardoni [a,*]

[a] CNRS UMR7275, Inserm U1323, Université Côte d'Azur, Institut de Pharmacologie Moléculaire et Cellulaire, 06560 Valbonne, France
[b] Inserm U1194, Université Montpellier, Institut de Recherche en Cancérologie de Montpellier, 34298 Montpellier Cedex 5, France
[c] Department of Anatomical, Histological, Forensic and Orthopaedic Sciences, DAHFMO, Sapienza University of Rome, 00161 Rome, Italy
[d] Université Côte d'Azur, Centre Commun de Microscopie Appliquée, 06100 Nice, France
[e] Department of Life Science, University of Trieste, 34100 Trieste, Italy
[f] Department of Science, University Rome Tre, Rome, Italy
[g] Institute of Biochemistry and Cell Biology, IBBC-CNR, 00015 Monterotondo Scalo, Rome, Italy

ARTICLE INFO

Keywords:
cAMP and cGMP pathways
PDE2A
Autism Spectrum disorder
Intellectual disability
Mouse model
mGluR-dependent LTD

ABSTRACT

Phosphodiesterase 2 A (PDE2A) is an enzyme involved in the homeostasis of cAMP and cGMP and is the most highly expressed PDE in human brain regions critical for socio-cognitive behavior. In cerebral cortex and hippocampus, PDE2A expression level is upregulated in *Fmr1*-KO mice, a model of the Fragile X Syndrome (FXS), the most common form of inherited intellectual disability (ID) and autism spectrum disorder (ASD). Indeed, PDE2A translation is negatively modulated by FMRP, whose functional absence causes FXS. While the pharmacological inhibition of PDE2A has been associated to its pro-cognitive role in normal animals and in models of ID and ASD, homozygous *PDE2A* mutations have been identified in patients affected by ID, ASD and epilepsy. To clarify this apparent paradox about the role of PDE2A in brain development, we characterized here *Pde2a*$^{+/-}$ mice (homozygote animals being not viable) at the behavioral, cellular, molecular and electrophysiological levels. *Pde2a*$^{+/-}$ females display a milder form of the disorder with reduced cognitive performance in adulthood, conversely males show severe socio-cognitive deficits throughout their life. In males, these phenotypes are associated with microglia activation, elevated glutathione levels and increased externalization of Glutamate receptor (GluR1) in CA1, producing reduced mGluR-dependent Long-term Depression. Overall, our results reveal molecular targets of the PDE2A-dependent pathway underlying socio-cognitive performance. These results clarify the mechanism of action of pro-cognitive drugs based on PDE2A inactivation, which have been shown to be promising therapeutic approaches for Alzheimer's disease, schizophrenia, FXS as well as other forms of ASD.

Abbreviations: AMPAR, α-amino-3-hydroxy-5-methyl-4-isoxazolepropionic acid receptor; ASD, Autism spectrum disorder; cAMP, cyclic adenosine monophosphate; cGMP, cyclic guanosine monophosphate; DBD, developmental brain disorder; DIV, days *in vitro*; DL, dark-light; EZM, elevated zero maze; fEPSPs, filed excitatory postsynaptic potentials; FXS, Fragile X Syndrome; GAF, cGMP-binding; PDE, Anabaena adenylyl cyclases, *E. coli* FhlAs; GluR1, Glutamate receptor; ID, Intellectual disability; LTD, long-term depression; NO, nitric oxide; NOR, novel object recognition; PDE2A, Phosphodiesterase 2 A; PND, postnatal day; PP1, protein phosphatase-1; SCZ, schizophrenia; WT, wild type.

* Corresponding author.
E-mail address: bardoni@ipmc.cnrs.fr (B. Bardoni).
[1] Present Address : Dep. Bioanalysis Syneos Health Sophia-Antipolis thomas.maurin@syneoshealth.com

https://doi.org/10.1016/j.nbd.2023.106393
Received 29 November 2023; Received in revised form 21 December 2023; Accepted 21 December 2023
Available online 26 December 2023

1. Introduction

Cyclic adenosine monophosphate (cAMP) and cyclic guanosine monophosphate (cGMP) are secondary messengers involved in numerous cellular pathways. They coordinate a multitude of pathophysiological processes *via* the specific activation of cAMP-dependent and cGMP-dependent protein kinases, PKA and PKG, respectively (Delhaye and Bardoni, 2021). The homeostasis of these secondary messengers is finely regulated both during their synthesis by adenylate cyclase and guanylate cyclase and during their degradation by members of the phosphodiesterase (PDE) superfamily of enzymes (Azevedo et al., 2014). Different PDEs are expressed in the brain to varying extent (Delhaye and Bardoni, 2021; Paes et al., 2021).

In neurons, cAMP plays a key role in synaptic transmission through short- and long-term mechanisms. cAMP acts directly on ligated-gated channel neurotransmission, neurotransmitter synthesis, storage, release, receptor sensitivity, cytoskeletal organization and remodeling, and neuronal growth and differentiation (Delhaye and Bardoni, 2021). cAMP is a well-known regulator of microglial function and activation (Ghosh et al., 2015; Ghosh et al., 2012; Ghosh et al., 2016), affecting microglial and macrophage polarization to pro-inflammatory or anti-inflammatory phenotypes (Crocetti et al., 2022). In addition, nitric oxide/cyclic guanosine monophosphate (NO/cGMP) signaling plays a key role in synaptic plasticity (Reyes-Harde et al., 1999) and neuroinflammation (Correia et al., 2021). Strong evidence indicates that the cGMP/PKG pathway is involved in the modulation of glial cell activity as well as in neuroinflammatory and neurodegenerative processes (Peixoto et al., 2015; Moretti et al., 2016).

Phosphodiesterase 2 A (PDE2A) is a dual-substrate enzyme that hydrolyzes both cAMP and cGMP by its three isoforms located in the cytosol, intracellular membranes, and mitochondria, respectively. cGMP binds to the cGMP-binding PDE, *Anabaena* adenylyl cyclases, *E. coli* FhlAs (GAF) domain of PDE2A and induces a conformational change, resulting in enhanced hydrolysis of cAMP and cGMP (Noyama and Maekawa, 2003; Monterisi et al., 2017; Russwurm et al., 2009). PDE2A is abundant in the brain being the most highly expressed PDE in the human hippocampus, frontal cortex, and striatum, all of which are essential for cognition and social interactions (Delhaye and Bardoni, 2021; Stephenson et al., 2012; Stephenson et al., 2009; Lakics et al., 2010). PDE2A is also localized in the axons and nerve terminals of principal neurons, and is the only PDE associated with docked synaptic vesicles (Boyken et al., 2013). Remarkably, about 50% of the total amount of hydrolyzed cGMP is PDE2A-dependent during rat brain synaptogenesis (Schiavi et al., 2022).

Inhibition of PDE2A is known to have pro-cognitive effects (Boess et al., 2004; Domek-Łopacińska and Strosznajder, 2008; Helal et al., 2018; Nakashima et al., 2018a; Rutten et al., 2007; Reneerkens et al., 2013; Bollen et al., 2015; Redrobe et al., 2014; Lueptow et al., 2016). Indeed, the administration of TAK-915, an inhibitor of PDE2A, to MK-801-treated rats, a schizophrenia model, reversed deficits in memory and social interaction in these animals (Nakashima et al., 2018b). In agreement with the "cAMP theory" (Kelley et al., 2007), improvement in memory and social interaction deficits were shown in Valproate-exposed rats, an environmental model of ASD, and in the *Fmr1*$^{-/y}$ mouse and rat, rodent models of Fragile X Syndrome (FXS) (Schiavi et al., 2022; Maurin et al., 2019) treated with another PDE2A specific inhibitor, Bay607550. Consistent with these findings, we showed increased expression and activation of PDE2A as a prominent characteristic of the pathophysiology of both these disorders (Maurin et al., 2018). Homozygous mutations in *PDE2A* have been found in patients with autism spectrum disorder (ASD) and intellectual disability (ID) ranging from moderate to severe (Doummar et al., 2020; Haidar et al., 2020; Salpietro et al., 2018; Yousaf et al., 2023). Moreover, reduced levels of PDE2A have been reported in *post-mortem* analyses of the amygdala and the frontal cortex obtained from patients affected by schizophrenia (SCZ) (Farmer et al., 2020).

To better define the role of PDE2A in neurodevelopment, we characterize here *Pde2a*$^{+/-}$ mice, since *Pde2a* knock-out in this species is lethal during embryogenesis (Stephenson et al., 2009). We show that these animals are a novel developmental brain disorder (DBD) model displaying socio-cognitive deficits in males during infancy, adolescence, and adulthood, while females display only a deficit in cognitive performance in adulthood. This disorder in males is also characterized by altered synaptic plasticity associated to an abnormal AMPA receptor (R) trafficking and microglia activation during pruning age.

2. Methods

2.1. Animals

The experiments were performed following the Animals in Research: Reporting *In Vivo* Experiments (ARRIVE) guidelines and the European Community Directive 2010/63/EU. The experiments were approved by the local ethics committee (Comité d'Ethique en Expérimentation Animale CIEPAL-AZUR N. 00788.01; APAFIS #39606–202,110,061,015,176 v8) and by the French Ministry of Research.

WT and *Pde2a*$^{+/-}$ mice were on a C57Bl/6 J background. Mutant mice (B6; 129P2-Pde2a < tm1Dgen>/H EM: 02366) were obtained from EMMA, UK (Stephenson et al., 2009) and were revitalized at Plaisant SRL (Rome, Italy). All animals used in behavioral experiments were littermate and were generated and housed in groups of six in standard laboratory conditions (22 °c, 55 ± 10% humidity, 12-h light/12-h dark diurnal cycles), with food and water provided *ad libitum*. Mice were weaned at the third postnatal week, chipped and genotyped by PCR at the end of the experiments. *Pde2a*$^{+/-}$ mice and WT alleles were detected by PCR assay in which three primers (see Supplementary Table 3) amplify a 247 bp fragment in WT and two fragments in *Pde2a*$^{+/-}$, the same one as in the WT and an additional 354 bp fragment.

2.2. Neuronal cultures and neurite length measurements

Primary cortical neurons were prepared from embryos at E14.5 obtained from pregnant C57Bl/6 J *Pde2a*$^{+/-}$ mice, as previously described (Maurin et al., 2019). After 48 h and fixation, neurons were labeled with anti-Tuj1 antibody and the size of individual growing neurites was manually measured using the Fiji software (https://fiji.sc), from the soma to the end of the neurite.

2.3. PDE2A activity assay

Half brains of 1-month old mice were collected and snap frozen in liquid nitrogen and stored at −80 °C. Frozen brains were then homogenized using a glass homogenizer (15 strokes, 4 °C) in 20 mM Tris-HCl buffer pH 7.2 containing 0.2 mM EGTA, 5 mM β-mercaptoethanol, 2% *v*/v antiprotease cocktail (Sigma–Aldrich), 1 mM PMSF, 5 mM $MgCl_2$, 0.1% v/v Triton X-100. The homogenates were centrifuged at 14.000 *g* for 30 min at 4 °C.

PDE activity was measured in the supernatant with the method described by Thompson and Appleman (Thompson and Appleman, 1971) in 60 mM Hepes pH 7.2, 0.1 mM EGTA, 5 mM $MgCl_2$, 0.5 mg/ml bovine serum albumin (BSA), and 30 μg/ml soybean trypsin inhibitor, in a final volume of 0.15 ml. To evaluate the enzymatic activity of PDE2A, the specific inhibitor Bay 607550 was added to the reaction mix at a final concentration of 0.1 μM, before the addition of the substrate. PDE2A activity was calculated as the difference between the total hydrolytic activity and the residual hydrolytic activity assayed in the presence of the specific inhibitor (Schiavi et al., 2022).

2.4. Behavioral tasks description

See supplementary information

2.5. Electrophysiology

See supplementary information

2.6. Protein extraction and Western blot

Protein extraction was carried our as previously described (Maurin et al., 2018). Samples were boiled at 95 °C, or not boiled when testing for Glutamate receptor (GluR1) expression. Samples were separated on NuPAGE Bis-Tris 4%–12% gels in MOPS buffer. Separated proteins were transferred to nitrocellulose membranes (Bio-Rad). Membranes were blocked with PBS-Tween (0.1%) and milk (5%), and incubated with primary antibodies overnight. Anti-GAPDH (Millipore, 1:5000), anti-PDE2A (Abcam, 1:1000), anti-GluR1 (Cell Signaling, 1:1000) and anti-Ser845-GluR1 (Cell Signaling, 1:1000) were used here. After secondary antibody incubation, membranes were revealed using Immobilon Western (Millipore). Protein bands intensity were quantified using ImageJ.

2.7. Biochemical measurements of surface GluR1

Hippocampal slices (300 μm) were prepared from one-month mice and immediately placed in ice-cold ACSF saturated with 95% oxygen (O_2) and 5% carbon dioxide (CO_2). Slices (8 to 10 per group) were equilibrated at room temperature for 2 h and then incubated with DHPG ((*S*)-3,5-Dihydroxyphenylglycine) (100 μmol/l) for 5 min. All treatments were carried out in the presence of D-AP5 (50 μmol/l). Drugs were removed by three washes in ACSF containing D-AP5 and left in the same buffer for an additional 40 min. Slices were washed once with ice-cold aCSF (5 min) and then incubated with Sulfo-NHS-SS-biotin (Pierce Chemical Company, Rockford, Illinois; 1 mg/ml in aCSF) for 30 min on ice. Excess of biotin was removed by two brief washes with 100 mmol/l glycine (in aCSF for 5 min) and two ACSF washes. Slices were then homogenized in the same lysis buffer, sonicated, and centrifuged at 14000 *g* for 15 min to remove nuclear material and cell debris. Protein concentration was determined by using the Bradford assay (Bio-Rad). Sixty micrograms of proteins were used to measure total GluR1 and sixty micrograms of biotinylated proteins were incubated with streptavidin beads (Pierce Chemical Company) on a head-over-head shaker overnight at 4 °C. Beads were washed three times with lysis buffer; bound proteins were eluted with loading buffer by boiling for 5 min. Total proteins and isolated biotinylated proteins were analyzed by Western blotting.

2.8. Transmission electronic microscopy

Mice were intracardially perfused with 10 ml of 2.5% glutaraldehyde in 0.1 M cacodylate buffer. Fixed mice brains were sliced (200 μm) on a vibratome. Small sections from the cortical regions and CA1 hippocampus were microdissected under binoculars and post-fixed 2 h in reduced 1% osmium tetroxide with 1% potassium ferrocyanide in 0.1 M cacodylate buffer to enhance the staining of membranes. Samples were rinsed in distilled water, dehydrated in increasing concentrations of acetone and lastly embedded in epoxy resin (EPON). Contrasted ultrathin sections (70 nm) with uranyl acetate and lead citrate were analyzed under a JEOL 1400 transmission electron microscope operating at 100 kV and mounted with a Morada Olympus CCD camera.

2.9. RNA extraction and RT-qPCR

Total RNA was extracted from 20 mg of frozen cerebral cortex and hippocampus using the RNeasy mini kit (Qiagen, #74104) according to the manufacturer's instructions. RNA was resuspended in 30 μl of nuclease-free H_2O and treated with Turbo DNAse (Thermofisher Scientific). For each experimental sample, 1 μg of RNA was added to the RT reaction, that was performed using the SuperScript IV synthesis kit (Invitrogen). Initial amplification was performed with a denaturation step for 5 min at 65 °C, followed by oligo(dT) annealing for 10 min at 23 °C, primer annealing for 10 min at 53 °C, and primer extension for 10 min at 80 °C. Upon completion of the cycling steps, the reactions were stored at −20 °C. Quantitative PCR (RT-qPCR) was performed on a light cycler 480 (Roche) with MasterMix SYBR Green (Roche) following the manufacturer's instructions. Primer sequences are listed in Supplementary Table 3.

2.10. Immunohistochemistry experiments

Mice were perfused intra-aortically with 4% PFA and brains were collected. Immunostaining was performed on 40-μm-thick brain floating sections of 13 days old pups. Rabbit anti-mouse IBA1 (1:300, #CP290A, Biocare Medical) and goat anti-rabbit secondary antibody conjugated with Alexa 594 (1:500, Molecular Probes, USA) were used. Sections were mounted in Vectashield solution (H-1000, Vector Laboratories). Images mosaics for cell counting IBA1 positive (+) cells were acquired with an inverted microscope for epifluorescence (Axiovert 200 M, Zeiss, Germany) through a 10×/0.45 objective. High-resolution images for morphometric analysis for IBA1 immunostaining were acquired with a Laser Scanner Confocal Microscope (TCS, SP5, Leica, Germany) through a 63×/1.4oil immersion objective with a z-step of 0.5 μm and a pixel size of 70 nm.

2.11. Image analysis

For analysis of mitochondrial morphology, ImageJ was used to measure manually the area of each clearly visible and distinguishable mitochondrion from three different mice per genotype. For measurement of microglial morphology, we used high resolution *z*-stack of cerebral cortex images using the Imaris software (Bitplane). After a surface rendering of each channel, we analyzed the morphology using the "Filament" plug-in.

2.12. Statistical analysis

Results are expressed as mean ± standard error of the mean (SEM). All statistical analyses were based on biological replicates. Appropriate statistical tests used for each experiment are described in the corresponding figure legends. All statistical analyses were carried out using GraphPad Prism v.10.0.

3. Results

3.1. PDE2A levels and activity are reduced in *Pde2a*$^{+/-}$ mice

Since *Pde2a*-KO mice are not viable and die *in utero* at E15.5 (Assenza et al., 2018), we decided to analyze heterozygous animals (*Pde2a*$^{+/-}$). The levels of PDE2A in the hippocampus and cerebral cortex of both male and female mice at one month of age were lower than those in wildtype (WT) mice, as shown by Western blot (WB) analysis (Fig. 1A-B and C, respectively). Consistent with this result, PDE2A specific activity (measured by degradation of cGMP in the presence of Bay607550) is 35% lower in *Pde2a*$^{+/-}$compared to WT mice at the same age (Fig. 1D). Reduced expression of PDE2A was also observed by WB in protein extracts obtained from the brains of *Pde2a*$^{+/-}$ mouse embryos at E14.5, compared to WT mice (Fig. 1E). To show the impact of reduced PDE2A levels, we measured the size of the first neurite after 2 days of neuronal culture *in vitro* (DIV). As expected from our previous studies (Maurin et al., 2019), this structure is longer in *Pde2a*$^{+/-}$ neurons compared to WT neurons (Fig. 1F-G).

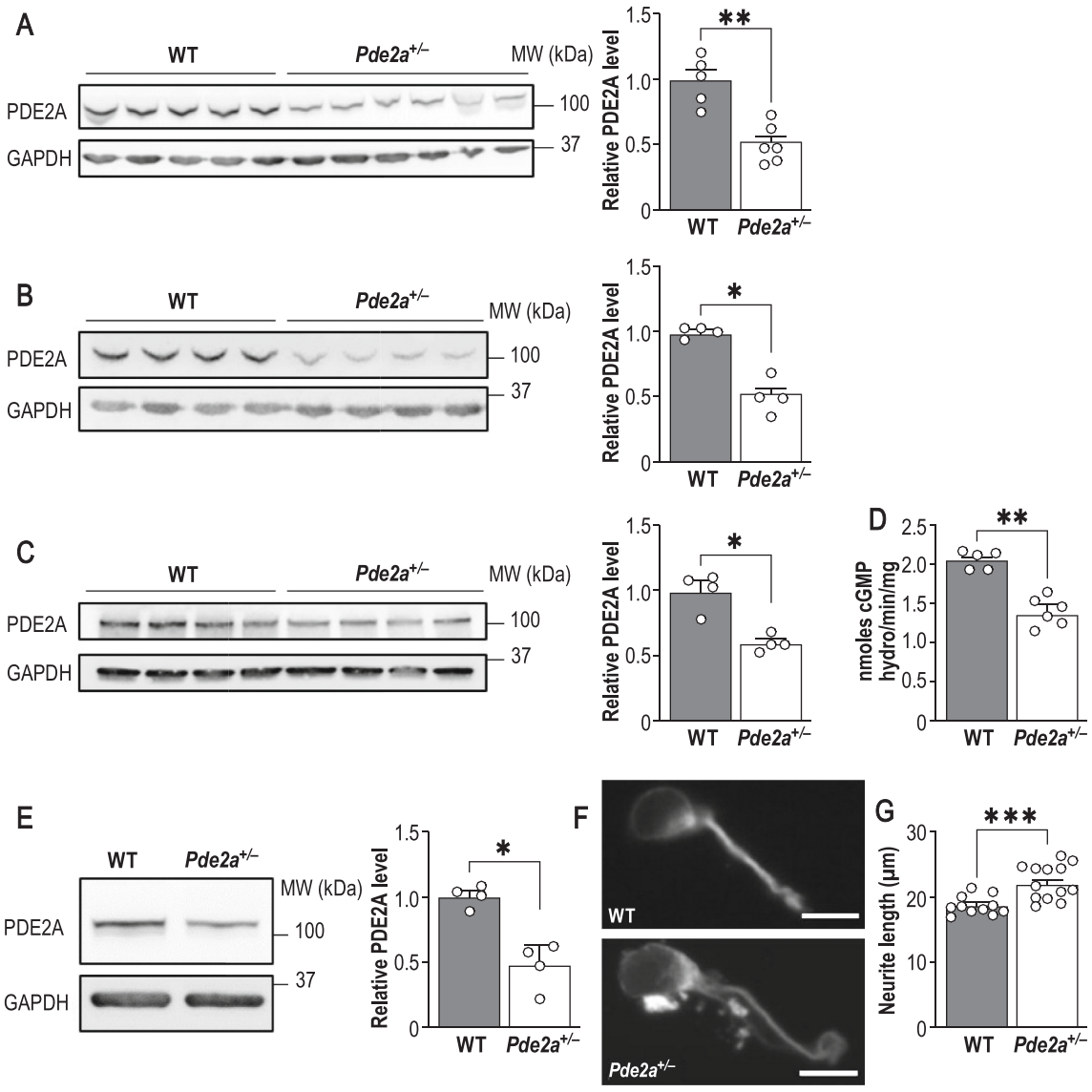

Fig. 1. PDE2A levels are correlated with neurite growth regulation.
(A,B) Representative Western Blot and quantification show reduced PDE2A levels in one-month male *Pde2a*$^{+/-}$ hippocampus and cerebral cortex (n = 4–6). (C) Representative Western Blot and quantification show reduced PDE2A levels in one-month female *Pde2a*$^{+/-}$ cerebral cortex (n = 4). (D) Specific PDE2A activity, measured by degradation of cGMP, is significantly reduced in *Pde2a*$^{+/-}$ compared to WT mice (n = 5–6). (E) Representative Western Blot and quantification show reduced PDE2A levels in *Pde2a*$^{+/-}$ cortical neurons at E14.5 compared to WT neurons (n = 3–4). (F) Representative pictures of 2 days *in vitro* cultured WT and *Pde2a*$^{+/-}$ primary cortical neurons (scale bar: 10 µm). (G) Histogram of neurite length showing longer neurite of *Pde2a*$^{+/-}$ neurons (n = 11–13). The data are represented as means ± SEM and analyzed using a Mann-Whitney test (adjusted p value: *$P < 0.05$, **$P < 0.01$, ***$P < 0.001$).

3.2. *Pde2a*$^{+/-}$ mice display deficits of socio-cognitive behaviors at infancy, adolescence and adulthood

We performed a behavioral characterization of *Pde2a*$^{+/-}$ mice of both sexes. Ultrasonic vocalizations (USVs) emitted by rodent pups in response to separation from the mother and nest play an essential communicative role in mother-offspring interactions (Mosienko et al., 2015). Isolation-induced USVs were collected for 3 min as social communication signals from mouse pups on postnatal day (PND) 10. *Pde2a*$^{+/-}$ pups emitted similar USVs than WT *Pde2a*$^{+/+}$ littermates (Fig. 2A). However, analyzing animals of different sex separately, male *Pde2a*$^{+/-}$ pups emitted a significant reduced number of UVS than WT male pups (Supplementary Fig. 1A). Body weight was measured to ensure that the reduced USVs were not the result of being physically smaller, because body weight is known to alter pup USV emissions (Mosienko et al., 2015). However, weight did not differ between the genotypes at 10 PND (Supplementary Fig. 1B), indicating normal growth in *Pde2a*$^{+/-}$ mice. The homing behavior test measures the tendency of rodent pups to maintain body contact with dams and siblings by discriminating the nest odor from a neutral odor (Melancia and Trezza, 2018). At PND 13, no differences between *Pde2a*$^{+/-}$ and WT were found in both sexes (Fig. 2B), but *Pde2a*$^{+/-}$ females display an increased latency in homing task compared with males having the same genotype (Fig. 2B). Adolescent male *Pde2a*$^{+/-}$ mice showed a reduced frequency of social interactions compared with their WT littermates, while female behave as controls (Fig. 2C). Overall, it appears that physiological PDE2A activity is critical for specific social behaviors, as *Pde2a*$^{+/-}$ pups displayed early communicative deficits but normal social discrimination ability. Only adolescent male animals showed reduced social interactions. Anxiety-like behavior was evaluated using elevated zero maze (EZM) tasks. Male *Pde2a*$^{+/-}$ mice, but not females, displayed a higher latency to exit from the closed arm of the maze (Fig. 2D, left panel), although the time spent in the open arms did not differ from that of the WT controls (Fig. 2D, right panel). The absence of anxiety-like

behavior was confirmed in male mice also by Dark/Light test (Supplementary Fig. 1C). We assessed learning and memory using a novel object recognition (NOR) task. We performed the test with a time of 5'min between the learning and test phases (Fig. 2E upper panels). *Pde2a*$^{+/-}$ mice of both sexes showed a significantly reduced discrimination index compared to WT littermates (Fig. 2E lower left panel), while the exploration time was the same for WT and *Pde2a*$^{+/-}$ mice during training (Supplementary Fig. 1D), and during the test phase (Fig. 2E lower right panel). *Pde2a*$^{+/-}$ females display a shorter exploration time compared with males (Supplementary Fig. 1D). Males were also tested by NOR waiting for 1 h between the training and the test (Supplementary Fig. 1E).

Since males appears more affected than females, we also assessed spatial memory in *Pde2a*$^{+/-}$ mice by using the Morris Water Maze task (Supplementary Fig. 2A). In the Cue phase (learning of the hidden platform's location with the help of visual cues), *Pde2a*$^{+/-}$ mice reached the visible platform at a significantly slower pace than WT mice on the first day of the experiment. During the second day, they had the same performance as WT mice (Supplementary Fig. 2B, left panel). During both the learning and probe phases, the performances of *Pde2a*$^{+/-}$ mice were comparable (Supplementary Fig. 2B, right panel; Fig. 2C, left panel). However, during the probe phase, *Pde2a*$^{+/-}$ mice spent significantly less time in the exact location of the platform (Fig. 2C, right panel) and in its surrounding zone. We studied male animal activity using actimetry and observed that mice of both genotypes crossed the beams detecting movement with the same frequency during the 68 h of the task (Supplementary Fig. 2D). During the same time, we observed that the number of rearings was not significantly different between WT and *Pde2a*$^{+/-}$ mice (Supplementary Fig. 2E), and animals of both genotypes had the same performance in the rotarod task (Supplementary Fig. 2F).

In conclusion, *Pde2a*$^{+/-}$ male mice display deficits in social interaction, working and short-term memory and, to a lesser extent, in spatial memory. Moreover, the behavior of these mice in the cue phase reinforces our interpretation that they have a delay in adaptation to novelty. *Pde2a*$^{+/-}$ females display only memory deficits in adulthood. No spontaneous seizures were observed in *Pde2a*$^{+/-}$ mice of both sexes.

Considering the milder phenotype in females during development, we decided to focus only on males to understand the molecular and cellular consequences of the reduction in PDE2A.

3.3. PDE2A genetic reduction results in multiple cellular abnormalities

We employed Golgi staining to study the morphology of dendritic spines in the brain of male *Pde2a*$^{+/-}$ mice. In the hippocampus, the length of dendritic spines displayed a small but statistically significant increase compared to that in the WT, while the number of spines did not differ between the two genotypes (Fig. 3A). Conversely, the length and number of dendritic spines in the cerebral cortex were reduced compared to those in the WT (Fig. 3B). This could be explained by an altered pruning process, which peaks two weeks after birth and is strongly correlated with microglial activity (Paolicelli et al., 2011; Cao et al., 2021). cAMP is a well-known regulator of microglial function and activation (Ghosh et al., 2015; Ghosh et al., 2012; Ghosh et al., 2016) and nitric oxide/cyclic guanosine monophosphate (NO/cGMP) signaling plays a key role in microglia activity and neuroinflammation (Correia et al., 2021; Peixoto et al., 2015; Moretti et al., 2016). In two-week-old *Pde2a*$^{+/-}$ mice, the number of cells expressing the microglia marker IBA1 was increased in the cerebral cortex compared to WT animals; however, it was normal in the hippocampus (Fig. 3C, Supplementary Fig. 3A). We confirmed these findings by Western blot, which showed an increased level of IBA1 in the cerebral cortex of two-week-old *Pde2a*$^{+/-}$ mice compared to that in WT mice (Supplementary Fig. 3B), but not at one month (Supplementary Fig. 3C). For further characterization, we studied the morphology of microglia in the cerebral cortex (Fig. 3D). Microglia are highly plastic cells whose morphological modifications indicate deregulation of their homeostasis. Confocal imaging revealed that the total length and number of filaments were increased in *Pde2a*$^{+/-}$ cerebral cortex compared to those in the WT (Fig. 3E-F). In addition, these cells were more ramified than the WT microglia (Fig. 3G), as assessed by Sholl analysis (Sholl, 1953). Using this approach, we also found that the number of microglia cells was higher in the cerebral cortex of *Pde2a*$^{+/-}$ mice (Supplementary Fig. 3D), which confirmed our observations (Fig. 3C).

Since microglial activation is one of the earliest features of nearly any change in brain physiology (Carson et al., 2006), we further investigated the abundance of cytokines and chemokines in the cerebral cortex and hippocampus using qPCR. TNF-α and IL-6, two pro-inflammatory cytokines, were upregulated in two-week-old *Pde2a*$^{+/-}$mice compared to WT mice, in the hippocampus and cerebral cortex, respectively (Fig. 3H-I), whereas CCL5 and CCL12 were not differently expressed in both regions. In four-week-old *Pde2a*$^{+/-}$ mice, TNF-α and IL-6 expression was increased in the hippocampus (Supplementary Fig. 3E), as opposed to what was observed in the cerebral cortex, where only CCL5 expression was significantly higher (Supplementary Fig. 3F). However, CCL5 was not differentially expressed in the hippocampus, and CCL12 was not expressed in the cerebral cortex at this age (Supplementary Fig. 3E-F).

3.4. Mitochondria and metabolism

A specific PDE2A isoform is localized in mitochondria (Monterisi et al., 2017) where it plays an important role in defining the morphology of those organelles (Monterisi et al., 2017; Lobo et al., 2020). Consistent with these findings, the presence of numerous thick and irregular mitochondria was reported in the fibroblasts of patients carrying a mutation in the *PDE2A* gene (Doummar et al., 2020). We studied the morphology of mitochondria using Transmission Electron Microscopy (TEM) images in one-month old WT and *Pde2a*$^{+/-}$ hippocampus and cerebral cortex (Fig. 4A). We observed that *Pde2a*$^{+/-}$ mitochondria were more electron-dense and their area was significantly decreased compared to WT in both the cerebral cortex and hippocampus (Fig. 4B-C).

Considering the critical role of mitochondria in cellular metabolism (Spinelli and Haigis, 2018), and the strong association existing between mitochondrial dysfunction and neuroinflammation (Bader and Winklhofer, 2020), we performed untargeted metabolomics of cerebral cortex extracts from WT and *Pde2a*$^{+/-}$ mice. The levels of L-tryptophan, a key amino acid implicated in serotonin synthesis, glutamate and of the related compounds gamma-glutamyl-glutamic acid, L-pyroglutamic acid, *N*-acetyl-aspartylglutamic acid and glutathione were increased in the cerebral cortex of *Pde2a*$^{+/-}$ compared to WT mice (Supplementary Table 1). Glutathione metabolism was the most dysregulated pathway in the *Pde2a*$^{+/-}$ mice cerebral cortex (Fig. 4D and Supplementary Table 2).

3.5. AMPA-dependent mGluR-dependent Long-Term Depression is disrupted in *Pde2a*$^{+/-}$ mice

We previously showed that the pharmacological inhibition of PDE2A by Bay607550 reduces the exaggerated mGluR-dependent Long-Term Depression (LTD) in the *Fmr1*-KO mouse CA1 (Maurin et al., 2019). At that time, we did not investigate the mechanism of action of PDE2A in the modulation of this synaptic plasticity, which can be now explored by using the *Pde2a*$^{+/-}$ mice. First, the hippocampal mGluR-dependent LTD was investigated in CA1 of WT and *Pde2a*$^{+/-}$ mice. Extracellular AMPA receptor-mediated field excitatory postsynaptic potentials (fEPSPs) were evoked from CA1 region of hippocampus after electrical stimulation of CA1. Bath application of DHPG, an agonist of group I mGluRs, (100 μM, 5 min) induced a mGluR-LTD that is weaker in *Pde2a*$^{+/-}$ mice when compared with WT mice (Fig. 5A-B). Since DHPG action induces the internalization of GluR1 *via* DARPP-32-PP1-dependent dephosphorylation of Ser845 (Snyder et al., 2000), we measured the ratio of surface/

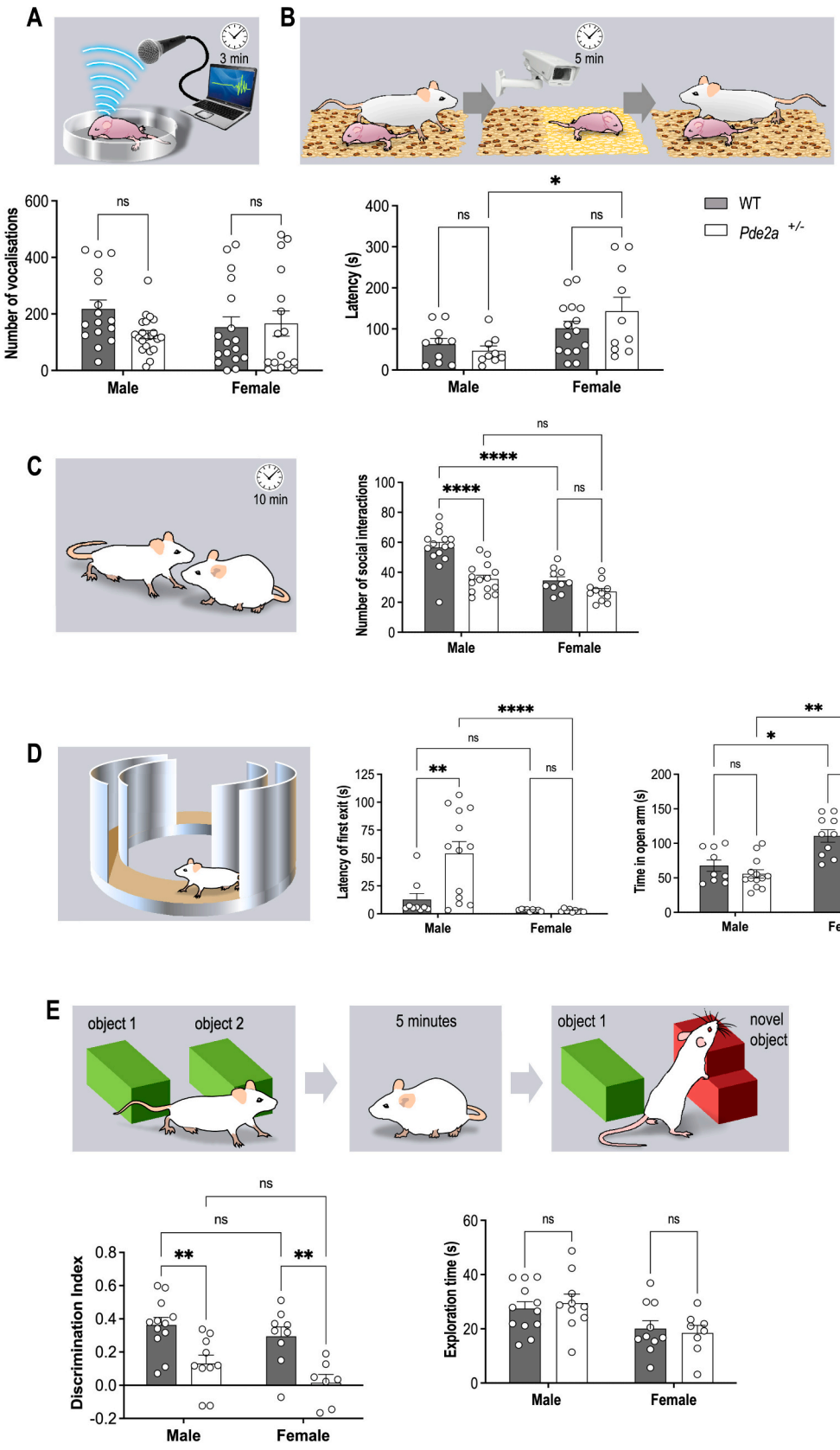

(caption on next page)

Fig. 2. : *Pde2a*$^{+/-}$ mice displayed deficits in various socio-cognitive tasks at different ages.
(A) Both male and female *Pde2a*$^{+/-}$ pups do not emit significantly less ultra-sonic vocalizations (USVs) when removed from the nest at P10. $F_{genotype\ (1,\ 66)} = 1.528$-$P = 0.2208$; $F_{sex\ (1,\ 66)} = 0.1538$ - $P = 0.6962$; $F_{genotype\times sex\ (1,\ 66)} = 2.610$ - $P = 0.1110$ (B) *Pde2a*$^{+/-}$ pups show no deficits in the homing test compared to WT pups at P13, as latency to reach the familiar litter and the time spent in it are not different. *Pde2a*$^{+/-}$ females are slower than *Pde2a*$^{+/-}$ males. $F_{genotype\ (1,\ 40)} = 0.3622$ - $P = 0.5507$; $F_{sex\ (1,\ 40)} = 10.02$ - P = 0,0030; $F_{genotype\times sex\ (1,\ 40)} = 1.806$ - $P = 0.1866$. (C) At one-month age, adolescent male *Pde2a*$^{+/-}$ mice make significantly less interaction when presented to a new mouse compared to WT, while female *Pde2a*$^{+/-}$ mice are not different from WT females. $F_{genotype\ (1,\ 47)} = 24.05$ - $P < 0.0001$; $F_{sex\ (1,\ 47)} = 27.67$ - $P < 0.0001$; $F_{genotype\times sex\ (1,\ 47)} = 5.504$; P = 0,0232. (D) At two-month age, adult male *Pde2a*$^{+/-}$ mice are significantly slower to first exit the closed arm from the zero-maze apparatus but not females at the same age. $F_{genotype\ (1,\ 36)} = 7.228$ - $P = 0.0108$; $F_{sex\ (1,\ 36)} = 16.02$ - $P = 0.0003$; $F_{genotype\times sex\ (1,\ 36)} = 7.635$ - $P = 0.0090$. Mice of both sexes spent the same amount of time in open arms at the end compared to WT mice. $F_{genotype\ (1,\ 37)} = 0.61$ - $P = 0.4381$; $F_{sex\ (1,\ 37)} = 25.1$ - $P < 0.0001$; $F_{genotype\times sex\ (1,\ 37)} = 0.22$ - $P = 0.6376$. (E) Male and female *Pde2a*$^{+/-}$ mice show significantly lower preference for a novel object than WT mice, with a diminution of discrimination index, whether with 5 min (Low - Left panel). $F_{genotype\ (1,\ 34)} = 23.85$ - $P < 0.0001$; $F_{sex\ (1,\ 34)} = 3.085$ - $P = 0.088$; $F_{genotype\times sex\ (1,\ 34)} = 0.2022$ - $P = 0.6558$. Male and female *Pde2a*$^{+/-}$ mice spent the same exploring time of objects than WT animals (Low-Right panel). $F_{genotype\ (1,\ 36)} = 0.00556$ - $P = 0.9410$; $F_{sex\ (1,\ 36)} = 9.797$ - $P = 0.0035$; $F_{genotype\times sex\ (1,\ 36)} = 0.3815$; $P = 0.5407$. The data are represented as means ± SEM and adjusted p value: *P < 0.05, **P < 0.01, **** $P < 0.0001$.

total GluR1 in hippocampal slices of four-week-old mice and we found that GluR1 receptors are localized at the membrane surface at higher levels in *Pde2a*$^{+/-}$ slices compared with WT after DHPG stimulation (Fig. 5C-D). This suggests an elevated abundance of GluR1 at the membrane upon DHPG. On the other side, it is known that the phosphorylation of is Ser845-GluR1 is cAMP/PKA dependent. We tested the level of GluR1 phosphorylation through WB using an antibody to monitor the phosphorylation of Ser845-GluR1 in hippocampus extracts of four-week-old WT and *Pde2a*$^{+/-}$ mice. We found increased phosphorylation of GluR1 (Fig. 5E-F) indicating an increased membrane abundance of GluR1 also at the steady-state condition in *Pde2a*$^{+/-}$ mouse hippocampus and, consequently, an altered responsiveness of AMPA receptor (R).

In summary, our results are consistent with an increased PDE2A-dependent abundance of cAMP impacting AMPAR trafficking.

4. Discussion

4.1. A sex-dependent phenotype

Mutations in *PDE2A* have been associated with DBD such as ID, ASD, epilepsy, and movement disorders in homozygous conditions (Yousaf et al., 2023). Only a few cases have been described; in some patients, the first neuropsychiatric evaluation was performed during adolescence or later (Doummar et al., 2020; Haidar et al., 2020; Salpietro et al., 2018; Yousaf et al., 2023). We present here the first characterization of *Pde2a*$^{+/-}$ mice as a model of this disorder since homozygote *Pde2a* mutant mice are embryonically lethal due to liver (Barbagallo et al., 2020) and heart defects (Assenza et al., 2018). *Pde2a*$^{+/-}$ mice displayed socio-cognitive deficits, as we assessed using multiple behavioral tasks. In particular, male *Pde2a*$^{+/-}$ pups displayed a better social discrimination at P13 (infancy) but reduced social interaction at P30 (adolescence) compared to female. Animals of both sexes exhibited memory impairments at P60 in the novel object recognition task but not of anxiety-like behaviors. Pde2a$^{+/-}$ males spent a higher latency to exit from the closed arm of the maze compared to females, suggesting a delay in adaptation to novelty not detected in females.

These data confirm the role of PDE2A in cognition, as previously suggested (Delhaye and Bardoni, 2021), but strongly highlight the role of this protein in male social interaction. It is then possible to hypothesize that there is a sex-dependent regulation of PDE2A, as with another PDE, PDE4D, which is differentially modulated in the male brain compared to the female brain (Zamarbide et al., 2019). *Pde2a*$^{+/-}$ female mice display a severe phenotype only at adulthood. This seems in line with the observation that females with ASD often camouflage the autistic core deficits with better social competences and they often have lower average intellectual abilities than males (Melancia et al., 2018). At the molecular point of view, these different behaviors can be explained by a sex-dependent compensatory mechanism in young mice that is not maintained in adults. Indeed, for instance, the partial loss of *Gabrb3* that differentially alters cerebellar physiology in young females but only at the adult age in male by the aforementioned sex-dependent compensation (Mercer et al., 2016).

No epileptic seizures or abnormal movement disorders were observed in infant, adolescent, or young adult *Pde2a*$^{+/-}$ animals of both sexes. This is different from what was described in patients carrying homozygote mutated forms of *PDE2A*. A rotarod test performed at 6 months did not show any phenotype in male or female *Pde2a*$^{+/-}$ mice. The fact that homozygous mutations are not lethal in patients suggests the presence of residual activity of PDE2A in these individuals, or, more likely, that its total absence is compensated for in the human liver and heart by the activity of another PDE, but this is not the case in mice. This compensation could also be present in the brains of those patients, since heterozygote individuals are not described as being affected by ASD or ID, indeed no neuropsychiatric evaluation was reported for the patients' parents carrying a heterozygous *PDE2A* mutation. However, only limited functional analyses of PDE2A mutant proteins identified in patients have been performed, and in some cases a poor description of the genetic variants has been reported. The endogenous activity of PDE2A was not measured in these patients (Doummar et al., 2020; Haidar et al., 2020; Salpietro et al., 2018; Yousaf et al., 2023). Consequently, we could not assess whether the variants identified thus far were gain- or loss-of-function mutations. Interestingly, even if we can consider the characterization of patients carrying mutations in *PDE2A* as preliminary, we noticed that for two female patients a regression of the neurodevelopmental phenotype was described (Haidar et al., 2020), leading to the possible speculation that in these patients a sex-specific phenotype is detectable in early infancy.

4.2. *Pde2a*$^{+/-}$ mice: cellular and molecular phenotypes in brain

In the analysis of *Pde2a*$^{+/-}$ mice, we focused on the role of PDE2A in hippocampus and cerebral cortex, the two brain regions where the translation of its mRNA is negatively modulated by FMRP (Delhaye and Bardoni, 2021; Maurin et al., 2019; Maurin et al., 2018). This reason, together with the mild neurodevelopmental phenotype of female *Pde2a*$^{+/-}$ mice, pushed us to carry out the molecular and cellular characterization of the brain lacking PDE2A only in male animals.

4.2.1. Microglia

A large body of literature has reported the implications of cAMP and cGMP in neuroinflammation (Ghosh et al., 2015; Ghosh et al., 2012; Ghosh et al., 2016). We found an increased number of IBA1+ cells associated with altered cell morphology only in the cerebral cortex from two-week-old *Pde2a*$^{+/-}$ mice, but no differences were observed in the hippocampus of the same mice. Increased expression levels of IL-6 and TNF-α were present in both the cerebral cortex and hippocampus of *Pde2a*$^{+/-}$ mice during development. Elevated expression of these cytokines is associated with ASD and schizophrenia (Ferencova et al., 2023; Goldsmith et al., 2016). Furthermore, the altered morphology of microglia observed in the cerebral cortex during the developmental pruning peak may explain the reduced number of dendritic spines

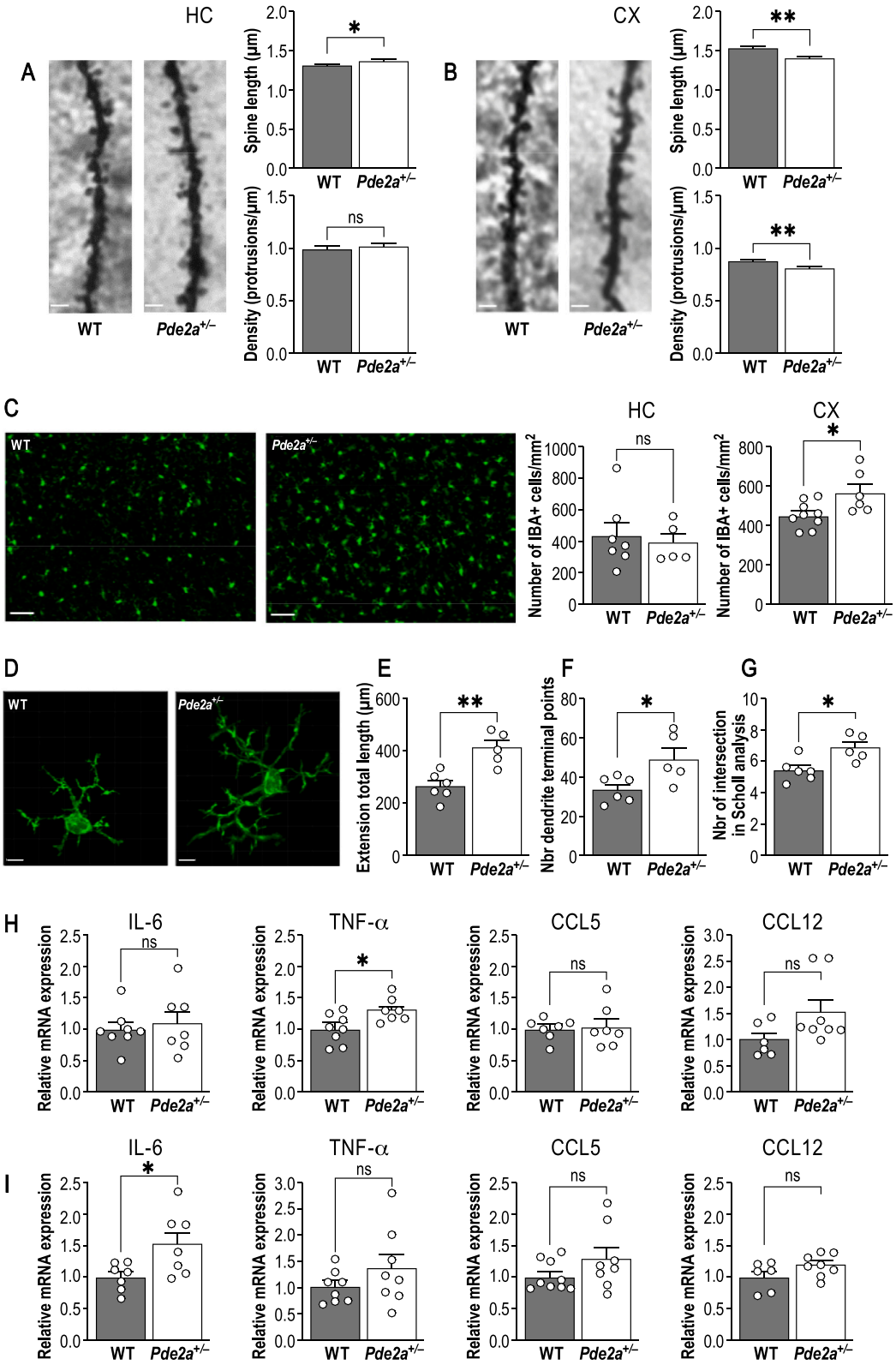

Fig. 3. : *Pde2a*$^{+/-}$ mice present dendritic spine and microglia morphology alteration, associated with pro-inflammation markers.
(A) Dendritic spines are significantly longer in CA1 of *Pde2a*$^{+/-}$ hippocampus while spine density is not different compared to WT. (B) Dendritic spine length and density are significantly reduced in the cerebral cortex of one-month *Pde2a*$^{+/-}$ mice (bar scale: 2 µm). (C) Representative image of IBA1 positive cells in WT and *Pde2a*$^{+/-}$ cerebral cortex at P13 (bar scale: 25 µm) showing that number of IBA1 positive cells in hippocampus are not different between WT and Pde2a+/− mice (n = 5–7), while in cerebral cortex *Pde2a*$^{+/-}$ mice have significantly more IBA1+ cells (*n* = 6–9). (D) Representative pictures of IBA1 immunoreactive microglia in WT and *Pde2a*$^{+/-}$ cerebral cortex at P13 (bar scale: 4 µm). (E) *Pde2a*$^{+/-}$ microglia present significantly higher extension total length, (F) more dendrite terminal points (G) and is wider, as it crossed more Scholl intersections (n = 5–6). (H,I) Relative mRNA expression of various inflammatory markers in hippocampus and cerebral cortex of WT and *Pde2a*$^{+/-}$ mice at P13 (n = 6–9). The data are represented as means ± SEM and analyzed using Mann-Whitney test. (p value: *P < 0.05, **P < 0.01)

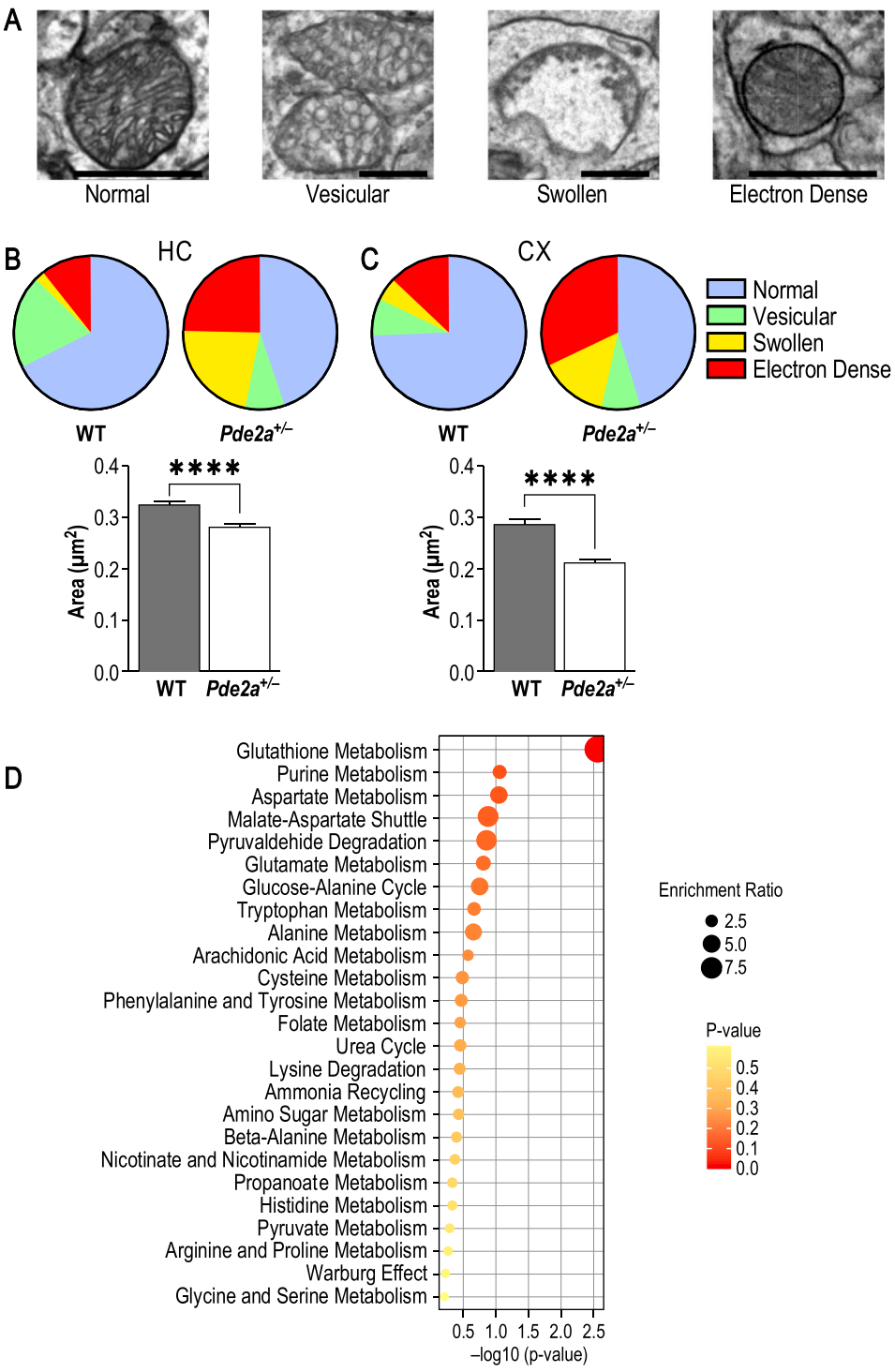

Fig. 4. : *Pde2a*$^{+/-}$ mice have abnormal mitochondria associated with metabolomics changes.
(A) Representative TEM images of four main mitochondrial morphology types (bar scale: 1 µm) (B,C) One-month-old *Pde2a*$^{+/-}$ mice presents abnormal mitochondria proportion and their mitochondria are significantly smaller in both hippocampus and cerebral cortex compared to WT mice. (D) Enrichment overview of metabolism pathways dysregulated in cerebral cortex of *Pde2a*$^{+/-}$ mice. The size and color of the dots indicate the enrichment ratio and the level of *P* value, respectively.The data are represented as means ± SEM and analyzed using the Mann-Whitney test (p value: ****P < 0.001)

observed in this brain region in one-month-old mice. Surprisingly, at one month of age, when we did not observe altered IBA1 expression, the expression level of IL-6 and TNF-α of *Pde2a*$^{+/-}$ mice was only increased in hippocampus but not in the cerebral cortex, where, conversely, we observed an increased abundance of CCL5. Interestingly, this chemokine has been described as a neuromodulator and its elevated expression has been found in patients with ASD (Ashwood et al., 2011; Shen et al., 2016). This result strongly suggests the need of to study the expression level of cytokines and chemokines during developmental age to monitor microglia plasticity in DBDs.

4.2.2. *Mitochondria and metabolism*

Mitochondria are indispensable organelles that play a crucial role in cellular energetics, metabolism, and survival (Spinelli and Haigis,

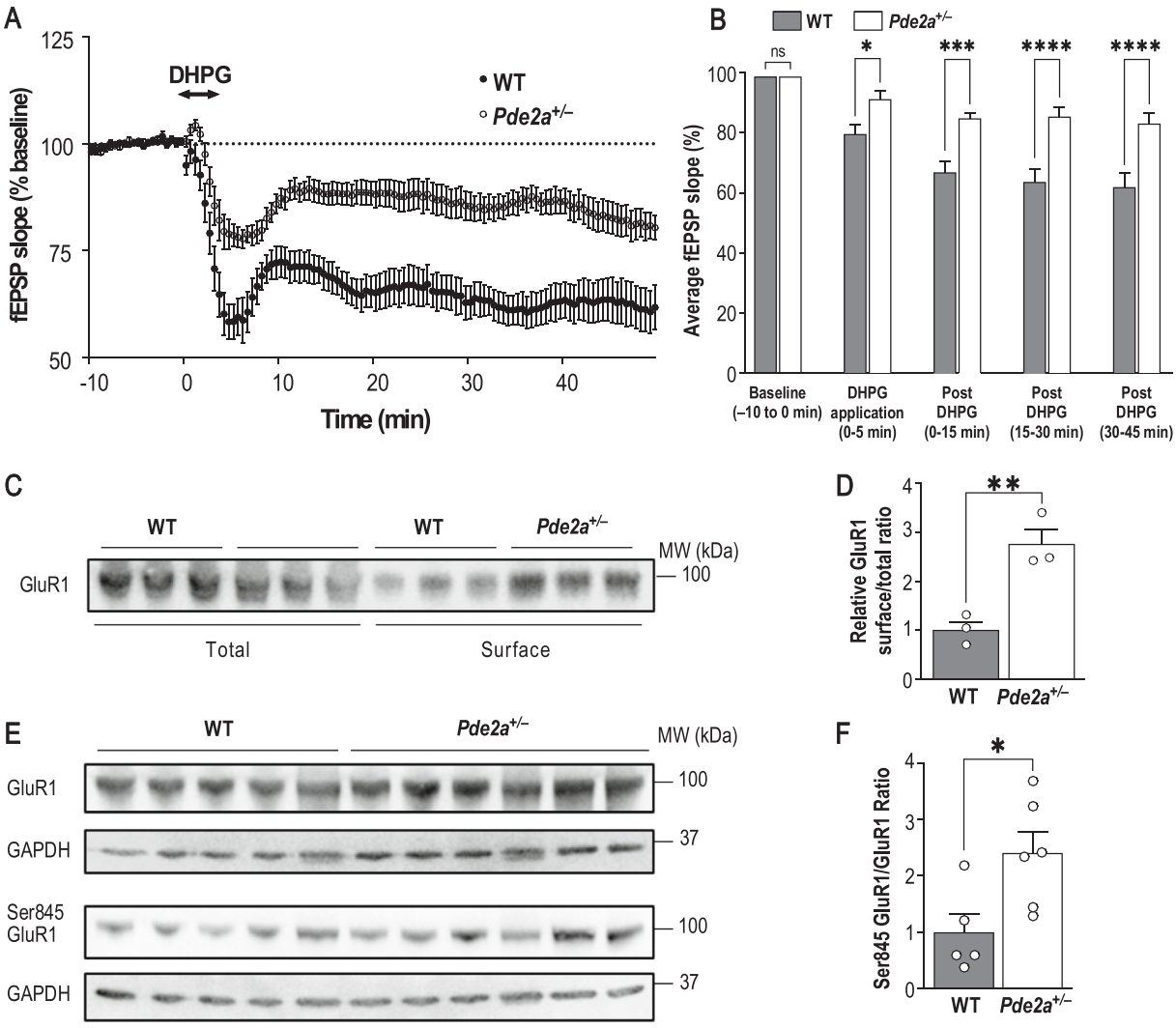

Fig. 5. Hippocampal mGluR-LTD is impaired in *Pde2a*$^{+/-}$ mice.
(A) DHPG (100 μM, 5 min) induced a mGluR-LTD of fEPSPs recorded from CA1 pyramidal neurons obtained from WT and *Pde2a*$^{+/-}$ mouse slices ($n = 10$). CA1 LTD induction was weaker in *Pde2a*$^{+/-}$ mice when compared to WT mice. (B) Bar graphs represent the average slope response during baseline (−10 to 0 min), DHPG application (0–5 min), 0–15 min after DHPG application, 15–30 min after DHPG application, 30–45 min after DHPG application. (C) Western Blot and (D) quantification show increased GluR1 presence in surface after DHPG application in one-month *Pde2a*$^{+/-}$ hippocampus (n = 3). (E) Western Blot and (F) quantification show an increase phosphorylation ratio of GluR1 in *Pde2a*$^{+/-}$ hippocampus compared to WT (n = 5–6). GluR1 and Ser845 GluR1 were previously normalized by their respective GAPDH level. The data are represented as means ± SEM and analyzed using the Mann-Whitney test and *t*-test for D (p value: *P < 0.05, **P < 0.01, ***P < 0.0005).

2018). Accumulating evidence indicates that aberrant mitophagy, respiratory chain deficits, and oxidative stress resulting from mitochondrial dysfunction lead to aberrant neurodevelopment (Ortiz-González, 2021). Neurological disorders associated with mitochondrial dysfunction are often associated with epilepsy in children. Oxidative damage induces hyperexcitability by modifying the excitation/inhibition balance (Wesół-Kucharska et al., 2021). **This may contribute to epileptic conditions in patients carrying homozygous mutations in *PDE2A*.**

It has been reported that the mitochondrial isoform of PDE2A (PDE2A2) is mostly localized in the inner mitochondrial membrane and regulates mitochondrial fusion/fission (Monterisi et al., 2017) and mitophagy (Lobo et al., 2020). All these findings seem consistent with our data showing that the total mitochondrial area in the *Pde2a*$^{+/-}$ hippocampus and cerebral cortex is smaller and an increased number of abnormal mitochondria is observed in these tissues.

Mitochondrial dysfunction is also strongly associated with neuroinflammation (Noh et al., 2014). Microglial immune functions have a high energy demand, which is regulated by mitochondria (Fairley et al., 2021). Therefore, mitochondrial quality is important for cellular homeostasis (Culmsee et al., 2018). Interestingly, the most deregulated metabolites in the cerebral cortex of *Pde2a*$^{+/-}$ mice (glutathione and purine metabolism) are well known to contribute to oxidative stress (Tian et al., 2022). Recent studies have suggested that mitochondrial dysfunction, including mitochondrial DNA (mtDNA) damage, metabolic defects, and quality control disorders, precedes microglial activation and subsequent neuroinflammation (Li et al., 2022). In this context, mitochondrial alterations may be associated with microglial activation.

4.3. GluR1 trafficking and mGluR-dependent LTD

We have shown an increased phosphorylation level of S845-GluR1 in *Pde2a*$^{+/-}$ hippocampus. Even if S845-GluR1 phosphorylation is known to be PKA-dependent (Snyder et al., 2000; Man et al., 2007; Esteban et al., 2003), the implication of a specific PDE was to our knowledge never shown before in hippocampus. Overall, our results clearly demonstrate the critical role of PDE2A in hippocampal AMPAR

trafficking and suggest an abnormal responsiveness of AMPAR in the hippocampus of these animals. Indeed, upon DHPG stimulation, *Pde2a*$^{+/-}$ CA1 neurons display an increased externalization of GluR1 and a reduced mGluR-dependent LTD. It has also been shown that mGluR5 activation promotes GluR1 Ser- 845 phosphorylation *via* inactivation of protein phosphatase-1 (PP1) (Dell'Anno et al., 2013), which targets GluR1 Ser-845. Thus, our results suggest that in the presence of an elevated level of GluR1 Ser-845 phosphorylation (50% increase compared to WT- Fig. 5E-F) the inhibition of PP1 maintains elevated Ser-845 phosphorylation compared to WT with a consequent reduced AMPAR internalization and an impaired mGluR-dependent-LTD.

5. Conclusions

Pde2a$^{+/-}$ mice represent a new DBD model and a useful tool for understanding the altered trajectory of brain development in pathological conditions. We highlight here that PDE2A-altered levels have a negative impact on the socio-cognitive phenotype, both when increased and reduced, strongly suggesting that PDE2A is a Goldilocks factor and the right amount of this enzyme is needed in the cell. In other words, both the increased or decreased levels of PDE2A have negative impact on downstream pathways and their underlined behaviors. Multiple molecular and cellular phenotypes characterize the brain of these mice. Remarkably, similar to *Pde2a*$^{+/-}$ mice, other forms of DBDs, such as Phelan-McDermid (SHANK3) (Wang et al., 2016; Vicidomini et al., 2017), Tuberous Sclerosis (TSC1/TSC2) (Bateup et al., 2011; Auerbach et al., 2011), Cowden (PTEN) (Takeuchi et al., 2013), mTORC2 (Zhu et al., 2018), display an impaired mGluR5-dependent LTD. Consistent with our data, inhibition of *Tsc2*, *PTEN* or *mTORC2* resulted in increased PKA activity and the presence of longer neurites (Hisatsune et al., 2021; Wyatt et al., 2014). This finding suggests an involvement of PDE2A in the pathophysiology of these disorders.

Our results, contributing to deciphering the mechanism of action of PDE2A, also allow to make hypotheses about the specific mechanism of action of pro-cognitive drugs based on PDE2A inhibition (Delhaye and Bardoni, 2021; Boess et al., 2004), that have been proposed in preclinical studies to treat Alzheimer's disease (AD), Schizophrenia, ASD and FXS (Delhaye and Bardoni, 2021; Schiavi et al., 2022).

Supplementary data to this article can be found online at https://doi.org/10.1016/j.nbd.2023.106393.

Declaration of generative AI in scientific writing

Authors did not use AI and AI-assisted technologies in the writing process.

Funding

This study was Supported by Inserm, CNRS, Féderation Recherche sur le Cerveau (FRC), Fondation Jérôme Lejeune (1728/2018 to BB and 1944/2019 to EL), Agence Nationale de la Recherche (ANR-20-16–0016CE to BB and EL and ANR-23-16–0023CE-02 to BB) and Fondation de France (WB-2022-46003) to BB. SD was supported by Fédération Française pour la Recherche sur l'Epilepsie (FFRE). AT and TM were supported by Fraxa Research Foundation. S.L-G acknowledges the University's Electron Microscopy facility (Centre Commun de Microscopie Appliquée, Université Côte d'Azur) and MICA Imaging platform Côte d'Azur supported by Université Côte d'Azur, Conseil Régional Sud Est PACA, Conseil Départemental and Gis Ibisa.

CRediT authorship contribution statement

Sébastien Delhaye: Writing – original draft, Investigation, Funding acquisition, Formal analysis, Data curation. **Marielle Jarjat:** Writing – review & editing, Supervision, Methodology. **Asma Boulksibat:** Writing – review & editing, Methodology. **Clara Sanchez:** Writing – review & editing, Methodology. **Alessandra Tempio:** Writing – review & editing, Methodology. **Andrei Turtoi:** Writing – review & editing, Methodology, Formal analysis. **Mauro Giorgi:** Writing – review & editing, Methodology. **Sandra Lacas-Gervais:** Writing – review & editing, Methodology, Formal analysis. **Gabriele Baj:** Writing – review & editing, Methodology. **Carole Rovere:** Writing – review & editing, Supervision, Methodology. **Viviana Trezza:** Writing – review & editing, Methodology, Conceptualization. **Manuela Pellegrini:** Writing – review & editing, Resources, Conceptualization. **Thomas Maurin:** Writing – review & editing, Formal analysis, Conceptualization. **Enzo Lalli:** Writing – review & editing, Supervision, Funding acquisition, Formal analysis, Data curation. **Barbara Bardoni:** Writing – original draft, Validation, Supervision, Data curation, Conceptualization.

Declaration of Competing Interest

The authors declare no competing interests.

Acknowledgments

The authors are grateful to M. Capovilla for critical reading of the manuscript, A. Thomazeau, C. Gwizdek, I.Bethus and F. Naro for discussion. They are indebted to F. Aguila for graphical artwork and to C. Boscagli for technical help.

References

Ashwood, P., Krakowiak, P., Hertz-Picciotto, I., Hansen, R., Pessah, I.N., Van de Water, J., 2011. Associations of impaired behaviors with elevated plasma chemokines in autism spectrum disorders. J. Neuroimmunol. 232, 196–199. https://doi.org/10.1016/j.jneuroim.2010.10.025.

Assenza, M.R., Barbagallo, F., Barrios, F., Cornacchione, M., Campolo, F., Vivarelli, E., et al., 2018. Critical role of phosphodiesterase 2A in mouse congenital heart defects. Cardiovasc. Res. 114, 830–845. https://doi.org/10.1093/cvr/cvy030.

Auerbach, B., Osterweil, E., Bear, M., 2011. Mutations causing syndromic autism define an axis of synaptic pathophysiology. Nature. 480, 63–68. https://doi.org/10.1038/nature10658.

Azevedo, M.F., Faucz, F.R., Bimpaki, E., Horvath, A., Levy, I., de Alexandre, R.B., et al., 2014. Clinical and molecular genetics of the phosphodiesterases (PDEs). Endocr. Rev. 35, 195–233. https://doi.org/10.1210/er.2013-1053.

Bader, V., Winklhofer, K.F., 2020. Mitochondria at the interface between neurodegeneration and neuroinflammation. Semin. Cell Dev. Biol. 99, 163–171. https://doi.org/10.1016/j.semcdb.2019.05.028.

Barbagallo, F., Rotilio, V., Assenza, M.R., Aguanno, S., Orsini, T., Putti, S., et al., 2020. PDE2A is indispensable for mouse liver development and hematopoiesis. Int. J. Mol. Sci. 21, 2902. https://doi.org/10.3390/ijms21082902.

Bateup, H.S., Takasaki, K.T., Saulnier, J.L., Denefrio, C.L., Sabatini, B.L., 2011. Loss of Tsc1 in vivo impairs hippocampal mGluR-LTD and increases excitatory synaptic function. J. Neurosci. 31, 8862–8869. https://doi.org/10.1523/JNEUROSCI.1617-11.2011.

Boess, F.G., Hendrix, M., van der Staay, F.J., Erb, C., Schreiber, R., van Staveren, W., et al., 2004. Inhibition of phosphodiesterase 2 increases neuronal cGMP, synaptic plasticity and memory performance. Neuropharmacology. 47, 1081–1092. https://doi.org/10.1016/j.neuropharm.2004.07.040.

Bollen, E., Akkerman, S., Puzzo, D., Gulisano, W., Palmeri, A., D'Hooge, R., et al., 2015. Object memory enhancement by combining sub-efficacious doses of specific phosphodiesterase inhibitors. Neuropharmacology. 95, 361–366. https://doi.org/10.1016/j.neuropharm.2015.04.008.

Boyken, J., Grønborg, M., Riedel, D., Urlaub, H., Jahn, R., Chua, J.J.E., 2013. Molecular profiling of synaptic vesicle docking sites reveals novel proteins but few differences between glutamatergic and GABAergic synapses. Neuron. 78, 285–297. https://doi.org/10.1016/j.neuron.2013.02.027.

Cao, P., Chen, C., Liu, A., Shan, Q., Zhu, X., Jia, C., et al., 2021. Early-life inflammation promotes depressive symptoms in adolescence via microglial engulfment of dendritic spines. Neuron. 109, 2573–2589.e9. https://doi.org/10.1016/j.neuron.2021.06.012.

Carson, M.J., Thrash, J.C., Walter, B., 2006. The cellular response in neuroinflammation: the role of leukocytes, microglia and astrocytes in neuronal death and survival. Clin. Neurosci. Res. 6, 237–245. https://doi.org/10.1016/j.cnr.2006.09.004.

Correia, S.S., Liu, G., Jacobson, S., Bernier, S.G., Tobin, J.V., Schwartzkopf, C.D., et al., 2021. The CNS-penetrant soluble guanylate cyclase stimulator CYR119 attenuates markers of inflammation in the central nervous system. J. Neuroinflammation 18, 213. https://doi.org/10.1186/s12974-021-02275-z.

Crocetti, L., Floresta, G., Cilibrizzi, A., Giovannoni, M.P., 2022. An overview of PDE4 inhibitors in clinical trials: 2010 to early 2022. Molecules. 27, 4964. https://doi.org/10.3390/molecules27154964.

Culmsee, C., Michels, S., Scheu, S., Arolt, V., Dannlowski, U., Alferink, J., 2018. Mitochondria, microglia, and the immune system—how are they linked in affective disorders? Front. Psychol. 9, 739. https://doi.org/10.3389/fpsyt.2018.00739.
Delhaye, S., Bardoni, B., 2021. Role of phosphodiesterases in the pathophysiology of neurodevelopmental disorders. Mol. Psychiatry 26, 4570–4582. https://doi.org/10.1038/s41380-020-00997-9.
Dell'Anno, M.T., Pallottino, S., Fisone, G., 2013. mGlu5R promotes glutamate AMPA receptor phosphorylation via activation of PKA/DARPP-32 signaling in striatopallidal medium spiny neurons. Neuropharmacology. 66, 179–186. https://doi.org/10.1016/j.neuropharm.2012.03.025.
Domek-Łopacińska, K., Strosznajder, J.B., 2008. The effect of selective inhibition of cyclic GMP hydrolyzing phosphodiesterases 2 and 5 on learning and memory processes and nitric oxide synthase activity in brain during aging. Brain Res. 1216, 68–77. https://doi.org/10.1016/j.brainres.2008.02.108.
Doummar, D., Dentel, C., Lyautey, R., Metreau, J., Keren, B., Drouot, N., et al., 2020. Biallelic PDE2A variants: a new cause of syndromic paroxysmal dyskinesia. Eur. J. Hum. Genet. 28, 1403–1413. https://doi.org/10.1038/s41431-020-0641-9.
Esteban, J.A., Shi, S.H., Wilson, C., Nuriya, M., Huganir, R.L., Malinow, R., 2003. PKA phosphorylation of AMPA receptor subunits controls synaptic trafficking underlying plasticity. Nat. Neurosci. 6, 136–143. https://doi.org/10.1038/nn997.
Fairley, L.H., Wong, J.H., Barron, A.M., 2021. Mitochondrial regulation of microglial immunometabolism in Alzheimer's disease. Front. Immunol. 12, 624538 https://doi.org/10.3389/fimmu.2021.624538.
Farmer, R., Burbano, S.D., Patel, N.S., Sarmiento, A., Smith, A.J., Kelly, M.P., 2020. Phosphodiesterases PDE2A and PDE10A both change mRNA expression in the human brain with age, but only PDE2A changes in a region-specific manner with psychiatric disease. Cell. Signal. 70, 109592 https://doi.org/10.1016/j.cellsig.2020.109592.
Ferencova, N., Visnovcova, Z., Ondrejka, I., Hrtanek, I., Bujnakova, I., Kovacova, V., et al., 2023. Peripheral inflammatory markers in autism spectrum disorder and attention deficit/hyperactivity disorder at adolescent age. Int. J. Mol. Sci. 24, 11710. https://doi.org/10.3390/ijms241411710.
Ghosh, M., Garcia-Castillo, D., Aguirre, V., Golshani, R., Atkins, C.M., Bramlett, H.M., et al., 2012. Pro-inflammatory cytokine regulation of cyclic AMP-phosphodiesterase 4 signaling in microglia in vitro and following CNS injury. Glia. 60, 1839–1859. https://doi.org/10.1155/2015/308461.
Ghosh, M., Aguirre, V., Wai, K., Felfly, H., Dietrich, W.D., Pearse, D.D., 2015. The interplay between cyclic AMP, MAPK, and NF-κB pathways in response to proinflammatory signals in microglia. Biomed. Res. Int. 2015, 308461 https://doi.org/10.1155/2015/308461.
Ghosh, M., Xu, Y., Pearse, D.D., 2016. Cyclic AMP is a key regulator of M1 to M2a phenotypic conversion of microglia in the presence of Th2 cytokines. J. Neuroinflammation 13, 9. https://doi.org/10.1186/s12974-015-0463-9.
Goldsmith, D., Rapaport, M., Miller, B., 2016. A meta-analysis of blood cytokine network alterations in psychiatric patients: comparisons between schizophrenia, bipolar disorder and depression. Mol. Psychiatry 21, 1696–1709. https://doi.org/10.1038/mp.2016.3.
Haidar, Z., Jalkh, N., Corbani, S., Abou-Ghoch, J., Fawaz, A., Mehawej, C., et al., 2020. A homozygous splicing mutation in PDE2A in a family with atypical Rett syndrome. Mov. Disord. 35, 896–899. https://doi.org/10.1002/mds.28023.
Helal, C.J., Arnold, E., Boyden, T., Chang, C., Chappie, T.A., Fisher, E., et al., 2018. Identification of a potent, highly selective, and brain penetrant phosphodiesterase 2A inhibitor clinical candidate. J. Med. Chem. 61, 1001–1018. https://doi.org/10.1021/acs.jmedchem.7b01466.
Hisatsune, C., Shimada, T., Miyamoto, A., Lee, A., Yamagata, K., 2021. Tuberous sclerosis complex (TSC) inactivation increases neuronal network activity by enhancing Ca2+ influx via L-type Ca2+ channels. J. Neurosci. 41, 8134–8149. https://doi.org/10.1523/JNEUROSCI.1930-20.2021.
Kelley, D.J., Davidson, R.J., Elliott, J.L., Lahvis, G.P., Yin, J.C.P., Bhattacharyya, A., 2007. The cyclic AMP cascade is altered in the fragile X nervous system. PLoS One 2, e931. https://doi.org/10.1371/journal.pone.0000931.
Lakics, V., Karran, E.H., Boess, F.G., 2010. Quantitative comparison of phosphodiesterase mRNA distribution in human brain and peripheral tissues. Neuropharmacology. 59, 367–374. https://doi.org/10.1016/j.neuropharm.2010.05.004.
Li, Y., Xia, X., Wang, Y., Zheng, J.C., 2022. Mitochondrial dysfunction in microglia: a novel perspective for pathogenesis of Alzheimer's disease. J. Neuroinflammation 19, 248. https://doi.org/10.1186/s12974-022-02613-9.
Lobo, M.J., Reverte-Salisa, L., Chao, Y.C., Koschinski, A., Gesellchen, F., Subramaniam, G., et al., 2020. Phosphodiesterase 2A2 regulates mitochondria clearance through Parkin-dependent mitophagy. Commun. Biol. 3, 596. https://doi.org/10.1038/s42003-020-01311-7.
Lueptow, L.M., Zhan, C.G., O'Donnell, J.M., 2016. Cyclic GMP–mediated memory enhancement in the object recognition test by inhibitors of phosphodiesterase-2 in mice. Psychopharmacology. 233, 447–456. https://doi.org/10.1007/s00213-015-4129-1.
Man, H.Y., Sekine-Aizawa, Y., Huganir, R.L., 2007. Regulation of α-amino-3-hydroxy-5-methyl-4-isoxazolepropionic acid receptor trafficking through PKA phosphorylation of the Glu receptor 1 subunit. Proc. Natl. Acad. Sci. 104, 3579–3584. https://doi.org/10.1073/pnas.0611698104.
Maurin, T., Lebrigand, K., Castagnola, S., Paquet, A., Jarjat, M., Popa, A., et al., 2018. HITS-CLIP in various brain areas reveals new targets and new modalities of RNA binding by fragile X mental retardation protein. Nucleic Acids Res. 46, 6344–6355. https://doi.org/10.1093/nar/gky267.
Maurin, T., Melancia, F., Jarjat, M., Castro, L., Costa, L., Delhaye, S., et al., 2019. Involvement of phosphodiesterase 2A activity in the pathophysiology of fragile X syndrome. Cereb. Cortex 29, 3241–3252. https://doi.org/10.1093/cercor/bhy192.
Melancia, F., Trezza, V., 2018. Modelling fragile X syndrome in the laboratory setting: a behavioral perspective. Behav. Brain Res. 350, 149–163. https://doi.org/10.1016/j.bbr.2018.04.042.
Melancia, F., Schiavi, S., Servadio, M., Cartocci, V., Campolongo, P., Palmery, M., et al., 2018. Sex-specific autistic endophenotypes induced by prenatal exposure to valproic acid involve anandamide signalling. Br. J. Pharmacol. 175, 3699–3712. https://doi.org/10.1111/bph.14435.
Mercer, A.A., Palarz, K.J., Tabatadze, N., Woolley, C.S., Raman, I.M., 2016. Sex differences in cerebellar synaptic transmission and sex-specific responses to autism-linked Gabrb3 mutations in mice. eLife. 5, e07596 https://doi.org/10.7554/eLife.07596.
Monterisi, S., Lobo, M.J., Livie, C., Castle, J.C., Weinberger, M., Baillie, G., et al., 2017. PDE2A2 regulates mitochondria morphology and apoptotic cell death via local modulation of cAMP/PKA signalling. eLife. 6, e21374 https://doi.org/10.7554/eLife.21374.
Moretti, R., Leger, P.L., Besson, V.C., Csaba, Z., Pansiot, J., Di Criscio, L., et al., 2016. Sildenafil, a cyclic GMP phosphodiesterase inhibitor, induces microglial modulation after focal ischemia in the neonatal mouse brain. J. Neuroinflammation 13, 95. https://doi.org/10.1186/s12974-016-0560-4.
Mosienko, V., Beis, D., Alenina, N., Wöhr, M., 2015. Reduced isolation-induced pup ultrasonic communication in mouse pups lacking brain serotonin. Mol. Autism. 6, 13. https://doi.org/10.1186/s13229-015-0003-6.
Nakashima, M., Imada, H., Shiraishi, E., Ito, Y., Suzuki, N., Miyamoto, M., et al., 2018a. Phosphodiesterase 2A inhibitor TAK-915 ameliorates cognitive impairments and social withdrawal in N-Methyl-d-aspartate receptor antagonist–induced rat models of schizophrenia. J. Pharmacol. Exp. Ther. 365, 179–188. https://doi.org/10.1124/jpet.117.245506.
Nakashima, M., Imada, H., Shiraishi, E., Ito, Y., Suzuki, N., Miyamoto, M., et al., 2018b. Phosphodiesterase 2A inhibitor TAK-915 ameliorates cognitive impairments and social withdrawal in N-methyl-d-aspartate receptor antagonist-induced rat models of schizophrenia. J. Pharmacol. Exp. Ther. 365, 179–188. https://doi.org/10.1124/jpet.117.245506.
Noh, H., Jeon, J., Seo, H., 2014. Systemic injection of LPS induces region-specific neuroinflammation and mitochondrial dysfunction in normal mouse brain. Neurochem. Int. 69, 35–40. https://doi.org/10.1016/j.neuint.2014.02.008.
Noyama, K., Maekawa, S., 2003. Localization of cyclic nucleotide phosphodiesterase 2 in the brain-derived Triton-insoluble low-density fraction (raft). Neurosci. Res. 45, 141–148. https://doi.org/10.1016/s0168-0102(02)00208-0.
Ortiz-González, X.R., 2021. Mitochondrial dysfunction: a common denominator in neurodevelopmental disorders? Dev. Neurosci. 43, 222–229. https://doi.org/10.1159/000517870.
Paes, D., Xie, K., Wheeler, D.G., Zook, D., Prickaerts, J., Peters, M., 2021. Inhibition of PDE2 and PDE4 synergistically improves memory consolidation processes. Neuropharmacology. 184, 108414 https://doi.org/10.1016/j.neuropharm.2020.108414.
Paolicelli, R.C., Bolasco, G., Pagani, F., Maggi, L., Scianni, M., Panzanelli, P., et al., 2011. Synaptic pruning by microglia is necessary for normal brain development. Science. 333, 1456–1458. https://doi.org/10.1126/science.1202529.
Peixoto, C.A., Nunes, A.K.S., Garcia-Osta, A., 2015. Phosphodiesterase-5 inhibitors: action on the signaling pathways of Neuroinflammation, neurodegeneration, and cognition. Mediat. Inflamm. 2015, 940207 https://doi.org/10.1155/2015/940207.
Redrobe, J.P., Jørgensen, M., Christoffersen, C.T., Montezinho, L.P., Bastlund, J.F., Carnerup, M., et al., 2014. In vitro and in vivo characterisation of Lu AF64280, a novel, brain penetrant phosphodiesterase (PDE) 2A inhibitor: potential relevance to cognitive deficits in schizophrenia. Psychopharmacology 231, 3151–3167. https://doi.org/10.1007/s00213-014-3492-7.
Reneerkens, O.A.H., Rutten, K., Bollen, E., Hage, T., Blokland, A., Steinbusch, H.W.M., et al., 2013. Inhibition of phoshodiesterase type 2 or type 10 reverses object memory deficits induced by scopolamine or MK-801. Behav. Brain Res. 236, 16–22. https://doi.org/10.1016/j.bbr.2012.08.019.
Reyes-Harde, M., Empson, R., Potter, B.V.L., Galione, A., Stanton, P.K., 1999. Evidence of a role for cyclic ADP-ribose in long-term synaptic depression in hippocampus. Proc. Natl. Acad. Sci. U. S. A. 96, 4061–4066. https://doi.org/10.1073/pnas.96.7.4061.
Russwurm, C., Zoidl, G., Koesling, D., Russwurm, M., 2009. Dual acylation of PDE2A splice variant 3. J. Biol. Chem. 284, 25782–25790. https://doi.org/10.1074/jbc.M109.017194.
Rutten, K., Prickaerts, J., Hendrix, M., van der Staay, F.J., Sik, A., Blokland, A., 2007. Time-dependent involvement of cAMP and cGMP in consolidation of object memory: studies using selective phosphodiesterase type 2, 4 and 5 inhibitors. Eur. J. Pharmacol. 558, 107–112. https://doi.org/10.1016/j.ejphar.2006.11.041.
Salpietro, V., Perez-Dueñas, B., Nakashima, K., San Antonio-Arce, V., Manole, A., Efthymiou, S., et al., 2018. A homozygous loss-of-function mutation in PDE2A associated to early-onset hereditary chorea. Mov. Disord. 33, 482–488. https://doi.org/10.1002/mds.27286.
Schiavi, S., Carbone, E., Melancia, F., di Masi, A., Jarjat, M., Brau, F., et al., 2022. Phosphodiesterase 2A inhibition corrects the aberrant behavioral traits observed in genetic and environmental preclinical models of autism Spectrum disorder. Transl. Psychiatry 12, 119. https://doi.org/10.1038/s41398-022-01885-2.
Shen, Y., Ji, Ou, Liu, M., Shi, L., Li, Y., Xiao, L., et al., 2016. Altered plasma levels of chemokines in autism and their association with social behaviors. Psychiatry Res. 244, 300–305. https://doi.org/10.18632/oncotarget.19326.
Sholl, D.A., 1953. Dendritic organization in the neurons of the visual and motor cortices of the cat. J. Anat. 87 (1), 387–406. https://www.ncbi.nlm.nih.gov/pmc/articles/PMC1244622/.
Snyder, G.L., Allen, P.B., Fienberg, A.A., Valle, C.G., Huganir, R.L., Nairn, A.C., et al., 2000. Regulation of phosphorylation of the GluR1 AMPA receptor in the neostriatum

by dopamine and psychostimulants in vivo. J. Neurosci. 20, 4480–4488. https://doi.org/10.1523/JNEUROSCI.20-12-04480.2000.
Spinelli, J.B., Haigis, M.C., 2018. The multifaceted contributions of mitochondria to cellular metabolism. Nat. Cell Biol. 20, 745–754. https://doi.org/10.1038/s41556-018-0124-1.
Stephenson, D.T., Coskran, T.M., Wilhelms, M.B., Adamowicz, W.O., O'Donnell, M.M., Muravnick, K.B., et al., 2009. Immunohistochemical localization of phosphodiesterase 2A in multiple mammalian species. J. Histochem. Cytochem. 57, 933–949. https://doi.org/10.1369/jhc.2009.953471.
Stephenson, D.T., Coskran, T.M., Kelly, M.P., Kleiman, R.J., Morton, D., O'neill, S.M., et al., 2012. The distribution of phosphodiesterase 2a in the rat brain. Neuroscience. 226, 145–155. https://doi.org/10.1016/j.neuroscience.2012.09.011.
Takeuchi, K., Gertner, M.J., Zhou, J., Parada, L.F., Bennett, M.V.L., Zukin, R.S., 2013. Dysregulation of synaptic plasticity precedes appearance of morphological defects in a Pten conditional knockout mouse model of autism. Proc. Natl. Acad. Sci. 110, 4738–4743. https://doi.org/10.1073/pnas.1222803110.
Thompson, W.J., Appleman, M.M., 1971. Multiple cyclic nucleotide phosphodiesterase activities from rat brain. Biochemistry. 10, 311–316. https://pubmed.ncbi.nlm.nih.gov/4321663/.
Tian, R., Yang, C., Chai, S.M., Guo, H., Seim, I., Yang, G., 2022. Evolutionary impacts of purine metabolism genes on mammalian oxidative stress adaptation. Zool. Res. 43, 241–254. https://doi.org/10.24272/j.issn.2095-8137.2021.420.
Vicidomini, C., Ponzoni, L., Lim, D., Schmeisser, M.J., Reim, D., Morello, N., et al., 2017. Pharmacological enhancement of mGlu5 receptors rescues behavioral deficits in SHANK3 knock-out mice. Mol. Psychiatry 22, 689–702. https://doi.org/10.1038/mp.2016.30.
Wang, X., Bey, A.L., Katz, B.M., Badea, A., Kim, N., David, L.K., et al., 2016. Altered mGluR5-Homer scaffolds and corticostriatal connectivity in a Shank3 complete knockout model of autism. Nat. Commun. 7, 11459. https://doi.org/10.1038/ncomms11459.
Wesół-Kucharska, D., Rokicki, D., Jezela-Stanek, A., 2021. Epilepsy in mitochondrial diseases—current state of knowledge on Aetiology and treatment. Children. 8, 532. https://doi.org/10.3390/children8070532.
Wyatt, L.A., Filbin, M.T., Keirstead, H.S., 2014. PTEN inhibition enhances neurite outgrowth in human embryonic stem cell–derived neuronal progenitor cells. J. Comp. Neurol. 522, 2741–2755. https://doi.org/10.1002/cne.23580.
Yousaf, H., Rehmat, S., Jameel, M., Ibrahim, R., Hashmi, S.N., Makhdoom, E.U.H., et al., 2023. A homozygous founder variant in PDE2A causes paroxysmal dyskinesia with intellectual disability. Clin. Genet. 104, 324–333. https://doi.org/10.1111/cge.14386.
Zamarbide, M., Mossa, A., Muñoz-Llancao, P., Wilkinson, M.K., Pond, H.L., Oaks, A.W., et al., 2019. Male-specific cAMP signaling in the hippocampus controls spatial memory deficits in a mouse model of autism and intellectual disability. Biol. Psychiatry 85, 760–768. https://doi.org/10.1016/j.biopsych.2018.12.013.
Zhu, P.J., Chen, C.J., Mays, J., Stoica, L., Costa-Mattioli, M., 2018. mTORC2, but not mTORC1, is required for hippocampal mGluR-LTD and associated behaviors. Nat. Neurosci. 21, 799–802. https://doi.org/10.1038/s41593-018-0156-7.